CARBON 50 (2012) 1690–1698

Available at www.sciencedirect.com

SciVerse ScienceDirect

journal homepage: www.elsevier.com/locate/carbon

Amorphous structural models for graphene oxides

Lizhao Liu [a,b], Lu Wang [a,b], Junfeng Gao [a,b], Jijun Zhao [a,b,*], Xingfa Gao [c], Zhongfang Chen [d]

[a] College of Advanced Science and Technology, Dalian University of Technology, Dalian 116024, China
[b] Key Laboratory of Materials Modification by Laser, Ion and Electron Beams, Dalian University of Technology, Ministry of Education, Dalian 116024, China
[c] Key Laboratory for Biomedical Effects of Nanomaterials and Nanosafety, Institute of High Energy Physics, Chinese Academy of Sciences, Beijing 100049, China
[d] Department of Chemistry, Institute for Functional Nanomaterials, University of Puerto Rico, San Juan, Puerto Rico 00931, USA

ARTICLE INFO

Article history:
Received 11 October 2011
Accepted 1 December 2011
Available online 8 December 2011

ABSTRACT

Based on the experimental observations, amorphous structural models of graphene oxides (GOs) were constructed and investigated by first-principles computations. Geometric structures, thermodynamic stabilities, and electron density of states of these amorphous GO models were examined and compared with the previously proposed ordered GO structures. The thermodynamically most favorable amorphous GO models always contain some locally ordered structures in the short range, due to a compromise of the formation of hydrogen bonds, the existence of dangling bonds, and the retention of the π bonds. Compared to the ordered counterparts, these amorphous GO structures possess good stability at low oxygen coverage. Varying the oxygen coverage and the ratio of epoxy and hydroxyl groups provides an efficient way to tune the electronic properties of the GO-based materials.

© 2011 Elsevier Ltd. All rights reserved.

1. Introduction

Since the synthesis in 2004 [1], graphene has demonstrated many excellent physical/chemical properties and held promise for a variety of applications [2–7]. In the family of graphene-based materials, graphene oxide (GO), a single layer of graphite oxide (first produced by treating graphite with strong aqueous oxidizing agents [8]), is also a focus of intensive studies partially because it is an important material to massively produce graphene [9–13]. More importantly, GO itself has manifested many unique properties that may lead to technological applications in many fields, such as electronic devices [14–17], chemical sensors [18,19], optical devices [20–24], energy storage [7,13,25,26], and composite materials [3,27].

Determining the atomic structure of GO is essential for a better understanding of its fundamental properties and for realization of the future technological applications. Over the past decade, various efforts have been given to solve this issue.

Among numerous experimental techniques, the most relevant one is the nuclear magnetic resonance (NMR) measurement [28–32]. The solid-state ^{13}C NMR and ^{1}H CPMAS NMR reveal the evidence of epoxy (C–O–C), hydroxyl (OH), carboxylic (COOH), and a small amount of other groups in GOs. However, it is extremely challenging to determine the detailed atomic structure of GO due to the following factors: (1) GO is a nonstoichiometric compound with a variety of compositions depending on its synthesis condition; (2) GO is strongly hydrophilic and hygroscopic; (3) GO is thermally unstable and slowly decomposes above 60–80 °C [31,33–35].

* *Corresponding author at:* College of Advanced Science and Technology, Dalian University of Technology, Dalian 116024, China. Fax: +86 411 84706100.
E-mail address: zhaojj@dlut.edu.cn (J. Zhao).
0008-6223/$ - see front matter © 2011 Elsevier Ltd. All rights reserved.
doi:10.1016/j.carbon.2011.12.014

In addition to NMR, various microscopic means were employed to characterize the atomic structures of GOs, including transmission electron microscopy (TEM) [34,36–40], scanning electron microscopy (SEM) [35,36], atomic force microscopy (AFM) [37,38,41–44], scanning tunneling microscopy (STM) [45]. Besides, measurements using optical analysis techniques [34–37,41–46], such as X-ray diffraction (XRD), X-ray photoelectron spectroscopy (XPS), Fourier transform infrared spectroscopy (FT-IR) and Raman spectroscopy, demonstrated that GO contains carbon atoms with different types of bonding states, for example, graphitic C, C–O–C, C–O, C=O, O–C=O, and so on.

Now it is generally accepted that GO bears hydroxyl and epoxy groups mostly on its basal plane [37,46]. The ratio of each bonding type of carbon can be tailored by the synthesis conditions, which enhances the complexity of atomic structure of GO. All these experimental observations suggest that the atomic structure of GO is nearly amorphous in large length scale.

Theoretically, many GO structural models have been proposed. Decades ago, four structural models respectively proposed by Hofmann and Holst [47], Ruess [48], Scholz and Boehm [49], Nakajima et al. [50,51], and Lerf and co-workers [30–32], were generally accepted, depending on the characterization technique prevalent at that time. Among them, the model proposed by Lerf and co-workers, in which the hydroxyl and epoxy groups distribute on the basal layer in a nearly disordered manner, explains the aforementioned experimental results very well. Recently, based on Cai's NMR experiment [46], Yan et al. [52,53] and our group [25,54] have identified the energetically favorable atomic configuration of GO, which contains epoxy and hydroxyl groups in close proximity with each other, and found that these functional groups prefer to aggregate. In addition to hydroxyl and epoxy, groups of epoxy pair and epoxy-hydroxyl pair in GO were also proposed by Zhang et al. [55]. Employing genetic algorithm and first-principles approaches, Xiang et al. [56] searched the most stable structure of oxidized graphene by considering various epoxy groups (normal epoxy, unzipped epoxy and epoxy pair), and found that phase separation between bare graphene and fully oxidized graphene is thermodynamically favorable in partially oxidized graphene, which agrees with our results [54]. Later, Lu et al. [57] found the long hydroxyl chains are not expected to be widely present in the real GO samples owing to their high chemical shifts according to the simulated NMR spectra.

Note that although the disordered GO models proposed by Hofmann and Holst [47], Ruess [48], Scholz and Boehm [49], Nakajima et al. [50,51], and Lerf et al. [30–32], are not thermodynamically most favorable, they can meet with the experimental observations to some extent; while the thermodynamically more favorable ordered GO models proposed recently are difficult to be synthesized. This leads to a plausible discrepancy between the experiments and theories: the structures of GOs are amorphous from experimental observations; but the ordered GO models are thermodynamically preferred from theoretical point of view.

To address this controversial issue and gain a deeper insight into the structural characteristics of GOs, here we considered the possibility of amorphous structural models for GOs and compared them with the ordered structures. It is interesting that the energetically preferred structures of our constructed amorphous GO models always exhibit some locally ordered structural motifs in the short range. Moreover, the energetically preferred amorphous GOs are nearly as stable as the ordered ones at low oxygen coverage. Our computations reveal an overall trend for the amorphous GO structures, which exhibit a locally ordered configuration but are disordered in the long range. These results not only are in line with the experimental observations of amorphous GOs, but also help understand the previous theoretical ordered models with lower energies.

2. Structural models and computational methods

2.1. *Amorphous GO models*

Our amorphous GO models start from a rectangular supercell of graphene consisting of 80 carbon atoms (17.21 Å × 12.45 Å in dimension). Based on the structural characteristics of the stable GO structures proposed by previous computations [25,52–56], we summarize the following rules to construct the amorphous structural models: (1) two functional groups cannot locate at the same carbon atom; (2) paired hydroxyl groups are added to two adjacent carbon atoms, one above and another below the graphene layer; (3) the numbers of the functional groups on each side of graphene sheet should be nearly equal to reduce the tension energy; (4) on one six-membered ring, more than four carbon atoms bonded with hydroxyl or five carbon atoms bonded with epoxy for each side of graphene basal is not allowed due to steric effect. For a given stoichiometry, certain numbers of epoxy and hydroxyl groups are randomly placed on the basal graphene layer according to the above rules.

By varying the numbers of epoxy and hydroxyl groups within the simulation supercell, amorphous GOs with different oxidation extents can be obtained. Here we define an oxygen coverage rate (R) as:

$$R = \text{number of sp}^3\text{ C (bonded with O or OH)/ total number of C atoms} \times 100\%.$$

In this work, we have constructed a series of amorphous GO models with R = 10% ($C_{80}O_6H_4$), 20% ($C_{80}O_{12}H_8$), 30% ($C_{80}O_{18}H_{12}$), 40% ($C_{80}O_{24}H_{16}$), 50% ($C_{80}O_{30}H_{20}$), 60% ($C_{80}O_{36}H_{24}$), and 70% ($C_{80}O_{42}H_{28}$), respectively. Note that for the amorphous GOs with different R, we assumed an OH:O ratio of 2.00, falling in the range of 1.06–3.25 in the experimental observations [58]. As a representative, one structural model of amorphous GO (R = 50%) is shown in Fig. 1a (top view) and Fig. 1b (side view). To be well considered, the amorphous GOs with the same coverage rate but different OH:O ratios are also investigated. Choosing a representative coverage of R = 50%, we constructed a series of models with OH:O = 0.22 ($C_{80}O_{22}H_4$), 0.50 ($C_{80}O_{24}H_8$), 0.86 ($C_{80}O_{26}H_{12}$), 1.33 ($C_{80}O_{28}H_{16}$), 2.00 ($C_{80}O_{30}H_{20}$), 3.00 ($C_{80}O_{32}H_{24}$), 4.67 ($C_{80}O_{34}H_{28}$), 8.00 ($C_{80}O_{36}H_{32}$), respectively.

For the ordered GOs, our previous work [25,54] showed that the epoxy and hydroxyl groups tend to locate and aggregate along the armchair direction from the energetic point of view. To compare with the amorphous GOs, we also assumed an

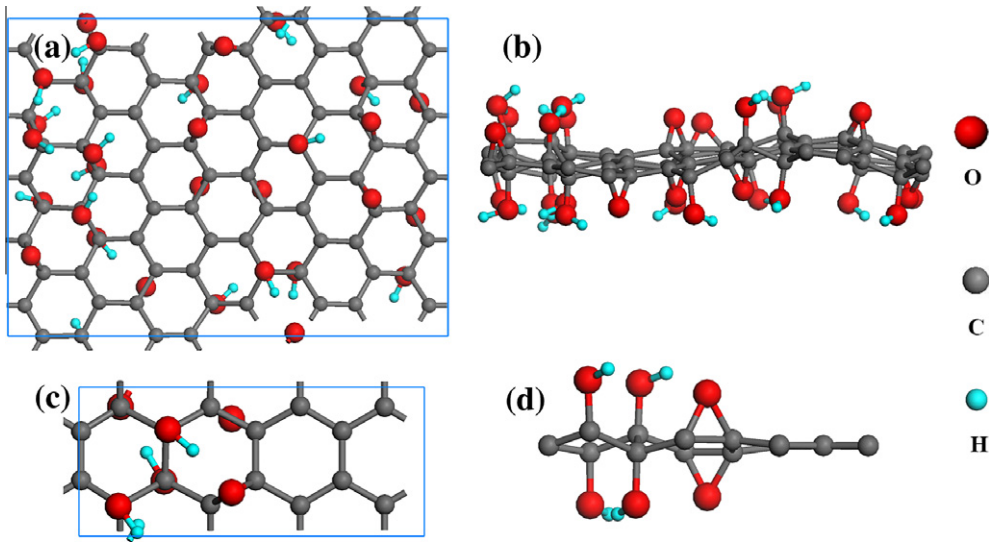

Fig. 1 – Representatively atomic structural models of GOs with R = 50% under optimization are presented, where (a) is top view and (b) is side view for the amorphous structure; (c) is top view and (d) is side view for the ordered structure, respectively. The red atom is O, the gray atom is C, and the light blue atom is H. (For interpretation of the references to colour in this figure legend, the reader is referred to the web version of this article.)

OH:O ratio of 2.00 in the ordered GOs. Hence, chain configuration composed of $h_2e_2^I$ motif in [54] was adopted to represent the ordered GO structure (top view in Fig. 1c and side view in Fig. 1d). In order to compare with their amorphous counterparts, ordered GO structural models with corresponding coverage of R = 10% ($C_{80}O_6H_4$), 20% ($C_{40}O_6H_4$), 33% ($C_{24}O_6H_4$), 40% ($C_{20}O_6H_4$), 50% ($C_{16}O_6H_4$), and 67% ($C_{12}O_6H_4$) were constructed by expanding the width of supercell with inclusion of only one $h_2e_2^I$ chain, and keeping pristine graphene as the rest part of the supercell.

2.2. *Computational methods*

Periodic first-principles computations were performed with the plane-wave pseudopotential technique implemented in the CASTEP program based on the density functional theory (DFT) [59,60]. The Perdew–Burke–Ernzerhof (PBE) functional in the generalized gradient approximation (GGA) was employed to describe the exchange–correlation energy [61]. The norm-conserving pseudopotentials [62] were adopted for describing the ion–electron interactions. A kinetic energy cut-off value of 600 eV was used. During the geometry optimization, the *k* space for amorphous GO was sampled by the Γ point, and the Monkhorst–Pack grids [63] with separation of 0.03 $Å^{-1}$ were chosen for the ordered GO supercell structures with different sizes. The supercell dimension perpendicular to the GO plane is chosen as 12 Å to avoid the interaction between the GO layer and its periodic images.

Within the basal plane of GO, both the supercell dimensions and the atomic coordinates of the initial configurations were fully relaxed. During optimization, dissociation of epoxy, formation and release of H_2O molecules, breaking of carbon-rings on the basal plane, and other structural damages were observed in some of the random GO configurations, especially for those with relatively high coverage rates (R ⩾ 30%). At the beginning, we have considered a large number of initial random structures (totally ~500) for coarse optimizations with lower SCF tolerance of total energy of 1.0×10^{-5} eV/atom. After that, for each coverage rate and OH:O ratio, we picked out ten energetically favorable configurations for further optimizations with higher SCF tolerance of total energy of 2.0×10^{-6} eV/atom. Note that these ten energetically favorable configurations are all locally stable without the above mentioned damages. Finally, the lowest-energy structure among the ten refined configurations was selected as the representative for discussions of structural and electronic properties.

3. Results and discussion

3.1. *Structural and electronic properties*

3.1.1. *OH:O = 2.00 with* **R = 10–70%**

In this part, we have considered the amorphous GOs with OH:O = 2.00 but different coverage rates. As an example, Fig. 2a displays the further optimized amorphous GO structure with R = 70%. Clearly the whole system is amorphous, but some ordered motifs exist in the short range, which are highlighted and shown individually on the top of the graph. After relaxation, the epoxy and hydroxyl groups in the highlighted parts are arranged in an ordered manner, i.e., aggregating along either armchair or zigzag directions. The armchair chain is similar to the $h_2e_2^I$ motif in ordered GO structure, taking the ordered GO with R = 40% as a representative in Fig. 2b. Moreover, these ordered fragments may aggregate. Such locally ordered motifs are also observed in the amorphous GOs with other coverage rates (R = 10–60%) in our structural models, which seem to be a universal feature.

This observation can be explained by a compromise of the formation of hydrogen bonds, the existence of dangling bonds, and the retention of the π bonds. When the functional groups aggregate, more hydrogen bonds will be formed to

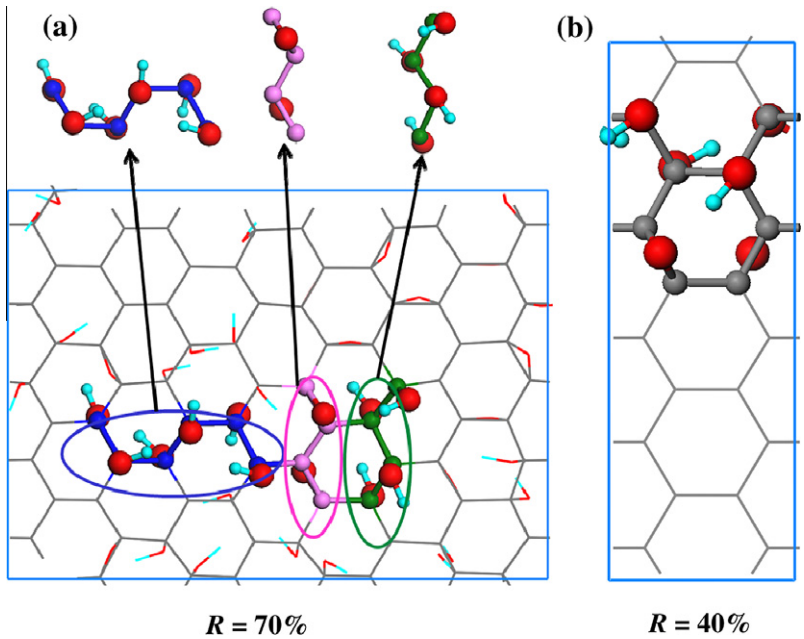

Fig. 2 – Optimized structures of GOs, (a) amorphous structure with R = 70% and (b) ordered structure with R = 40%, are presented. The highlighted parts in the amorphous GO (shown in the upper plot of graph (a)) are the locally ordered motifs.

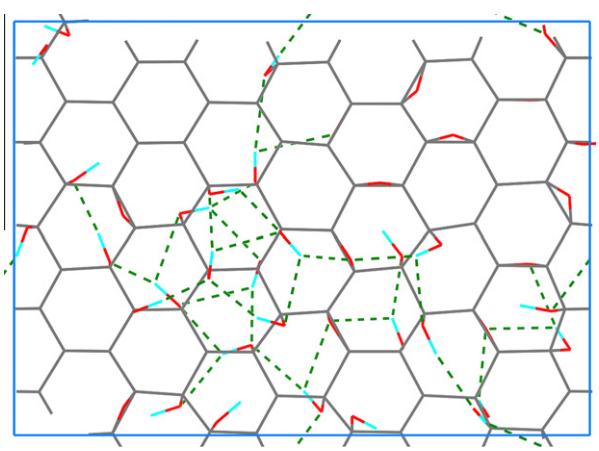

Fig. 3 – Hydrogen bonds in the amorphous GO with R = 70% are shown. The hydrogen bonds are highlighted by green dish lines. (For interpretation of the references to colour in this figure legend, the reader is referred to the web version of this article.)

lower the energy and stabilize the structure. Fig. 3 shows the hydrogen bonds in the structural model of Fig. 2a. Obviously, hydrogen bonding network is amassed in the vicinities of those three ordered parts (highlighted in Fig. 2a). Meanwhile, there are some dangling bonds (or unsaturated electrons) on the GO sheet, which are energetically unfavorable. Aggregation of epoxy and hydroxyl groups in an ordered way can efficiently eliminate these dangling bonds (or unsaturated electrons) by self-termination and thus to stabilize the GO structure. Reportedly, when the functional groups in the GO are assembled, large area of sp^2 carbon network will be separated from the sp^3 domain. This local phase separation will reduce the number of π bonds to be destroyed and is thermodynamically favorable as far as enthalpy is considered, as mentioned in [54,56].

Typically, GO is an insulator with a band gap of ~3 eV [38,53,64–66]. Its electronic properties can be effectively tuned by varying ratio of sp^2/sp^3 carbon bonds (concentration and relative ratio of the functional groups) on the basal plane [67]. By changing the oxidation level and the location of the oxidized region of GOs, Yan et al. [52,53] obtained variable band gaps from 0.2 to 4.2 eV using LDA calculations. Moreover, electrical conductivity of GOs is also tunable depending on the level of oxidation, and the magnitude of variation can be as high as $>10^6$ times [68]. In this work, we calculated the electron density of states (DOS) for both ordered and amorphous GO structures, aiming to reveal the correlation between electronic states and oxidation coverage. The theoretical DOS of ordered and amorphous GOs with R = 20%, 40%, and 50% are given in Fig. 4. As expected, the ordered GO structures always present a clean band gap. The band gaps of ordered GOs with R = 20%, 40%, and 50% are 1.22, 1.92 and 2.06 eV, respectively. For the ordered GOs, as the coverage rate increases, the band gap is widened due to increasing ratio of sp^3 carbon, which destroys the π-conjugated bonds on sp^2 graphene basal plane. On the contrary, as shown in Fig. 4 (right), DOS of the amorphous GOs usually exhibit some defective peaks around the Fermi level, which indicates existence of certain amount of dangling bonds in these disordered structures.

Here we define the minimum of conduction band contributed by sp^3 carbon as conduction-band minimum (CBM) and the maximum of valence band contributed by sp^3 carbon as valence-band maximum (VBM), respectively. There are some defect-induced states between CBM and VBM, which may originate from the unsaturated dangling bonds, structural distortion, and locally residual sp^2 and sp^2–sp^3 bonds. These defect-induced states are almost localized and may trap the

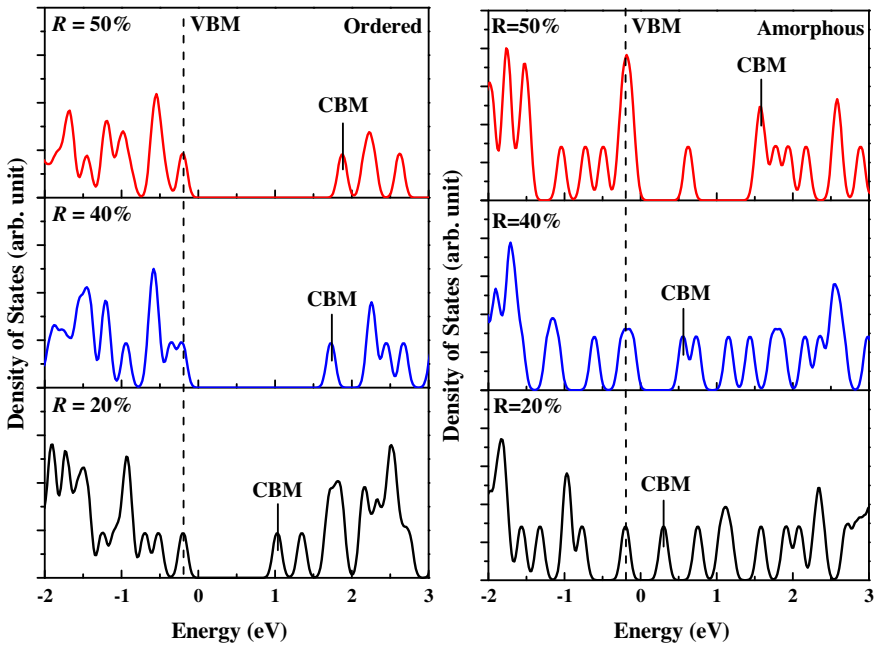

Fig. 4 – DOS of the ordered (left) and amorphous (right) GOs with different coverage rates R = 20%, 40%, 50% are plotted.

electrons so as to barely (or not) affect the electrical conductivity in real material applications [69]. If we ignore these mid-states and only consider the band gap between the CMB and VBM, the band gaps of amorphous GOs with R = 20%, 40%, and 50% are about 0.53, 0.80 and 1.77 eV, respectively. Hence, the trend of band gap for the amorphous GO structures with different coverage rate is also consistent with that for the ordered counterparts. Moreover, this trapping effect of defective states and trend of band gap versus coverage rate have been reported in previously experimental measurements [70].

3.1.2. R = 50% with OH:O ratio from 0.22 to 8.00

To further confirm our results, the amorphous GOs with R = 50% but different OH:O ratios are investigated. Two of the optimized GO structures are presented in Fig. 5 as representatives: one with abundant epoxy groups (OH:O = 0.22, upper plot), and the other with numerous hydroxyl groups with (OH:O = 8.00, lower plot). As highlighted in Fig. 5, the epoxy groups nearly form a chain in the epoxy-dominant upper structure (OH:O = 0.22), while there are also several locally ordered motifs in the lower one (OH:O = 8.00) with many hydroxyl groups. In other words, amorphous GO structures with different OH:O ratios also contain the locally ordered structures to enhance the thermodynamic stability. Thus, the stable amorphous structures of GOs from our random construction and first-principles relaxations exhibit disordered features in the long range but contain ordered structural motifs in the short range.

The DOS of amorphous GOs with different OH:O ratios of 0.50, 2.00, and 8.00 are displayed in Fig. 6. As the OH:O ratio increases, more electrons would transfer into the valence states. Again, the band gap between the CBM and VBM (ignoring the mid-states within the gap region) becomes larger as the OH:O ratio increases. The band gaps of amorphous GOs with OH:O ratio = 0.50, 2.00, and 8.00 are about 1.46, 1.76 and 2.45 eV, respectively.

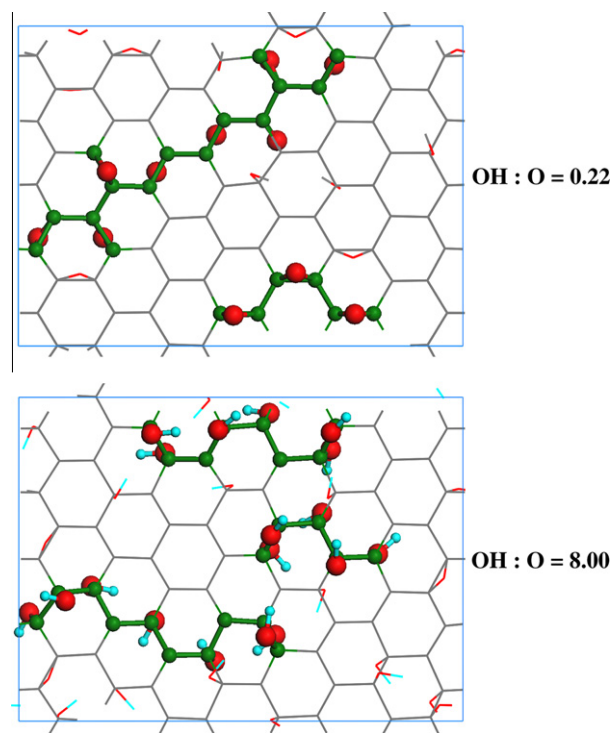

Fig. 5 – Amorphous GO structures with R = 50% but different OH:O ratios, (upper) OH:O = 0.22 and (lower) OH:O = 8.00, are presented. The locally ordered structures are highlighted by balls and sticks for the guide of eyes.

The increased band gap between the CBM and VBM with increasing OH:O ratio may be partially attributed to the hybridization of carbon atoms. Intuitionally, the carbon atom

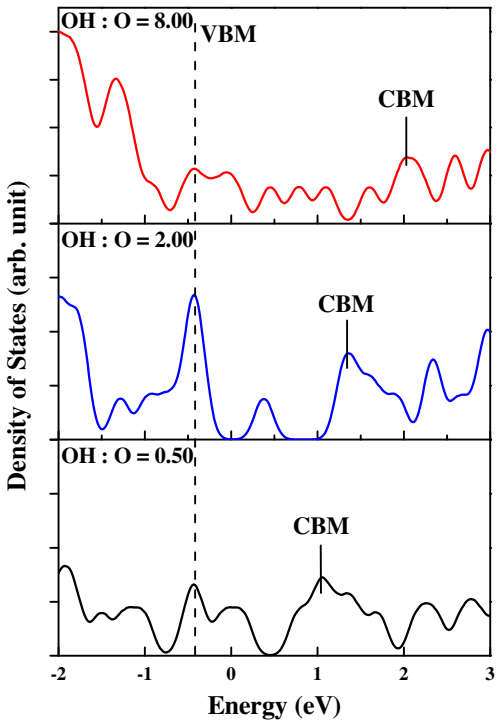

Fig. 6 – DOS of the amorphous GOs with different OH:O ratios (OH:O = 0.50, OH:O = 2.00, and OH:O = 8.00) are plotted.

bonded with a hydroxyl group has a larger bond angle (~105°) than that bonded with an epoxide group (~55°); thus the former is very close to that of ideal sp^3 hybridization state (109.47°). Therefore, carbon atoms in the GO structures with high OH:O ratio might be dominated by sp^3 hybridization, which would lead to a large band gap [52,71].

3.2. *Thermodynamic stability*

The thermodynamic stability of these amorphous and ordered GOs is discussed in terms of their formation energies. Here we define the heat of formation (H_f) from the total energies for all relevant systems using the following equation [54]:

$$H_f = E_{C_xO_yH_z}(GO) - xE_C(\text{graphene}) - y/2E_O(O_2) - z/2E_H(H_2),$$

where $E_{C_xO_yH_z}$ is the total energy of GO with the chemical formula of $C_xO_yH_z$, and E_C is the energy per carbon atom in graphene. E_O and E_H are the total energies of gaseous O_2 molecule and H_2 molecule, respectively.

The computed H_f for both amorphous and ordered GO structures are plotted as function of coverage rate R in Fig. 7. First, all H_f are negative, indicating that formation of GO through oxidation of graphene is an exothermic process, as found before [52–54,56]. Note that the heat of formation for those ordered GO structures varies linearly with R, which is a natural consequence of the chain-based supercell model used here. On the other hand, the H_f of amorphous GOs is not a straight line of oxidation rate R and it is higher than the H_f for the ordered ones by up to 0.19 eV per C atom. The energy difference between the amorphous and ordered GO structures reduces as the oxidation rate decreases. Extrapolation to low coverage limit shows that the amorphous GOs could be as

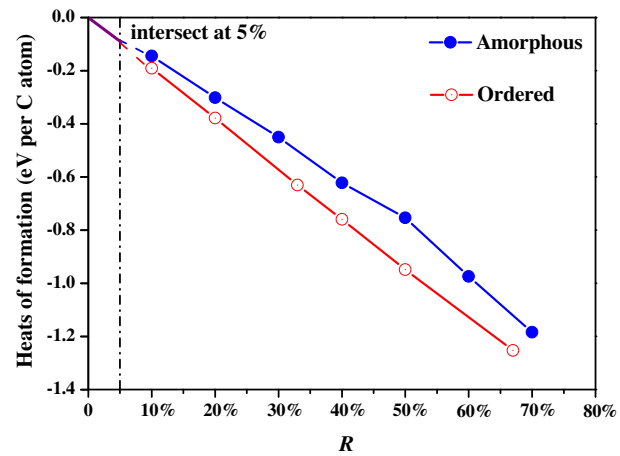

Fig. 7 – Heats of formation for the amorphous and ordered GO structures as function of coverage rate R are plotted.

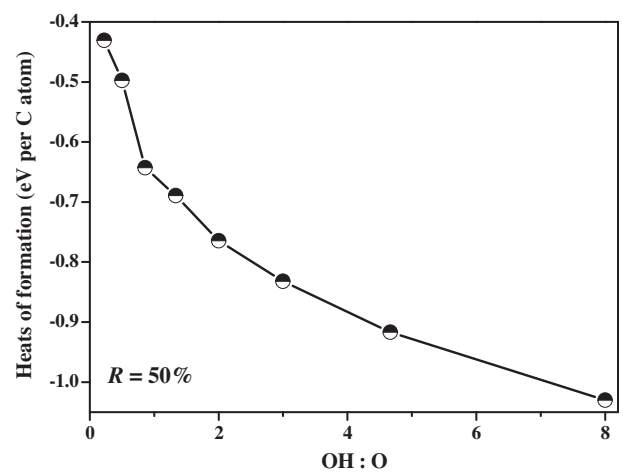

Fig. 8 – Heats of formation of the amorphous GOs with R = 50% but different OH:O ratios are plotted.

stable as the ordered GOs when coverage rate reaches below 5%. This result coincides with our previous theoretical work of kinetic analysis for GO formation (see Fig. 4 in [54]) that the homogenous GO phase is favored at low coverage, whereas inhomogeneous GO phase or phase separation is more likely to occur at relatively higher coverage.

The heats of formation for the amorphous GO structures with fixed R = 50% but different OH:O ratios are presented in Fig. 8. As the OH:O ratio increases, the heat of formation becomes lower and thus the GO system becomes thermodynamically more favorable. This result indicates that functionalization of hydroxyl groups on the GO sheet energetically prevails over epoxy groups, which is consistent with the previous theoretical results [52,53].

From the above discussions, we find that random configurations of GOs usually contain some locally ordered structural motifs and the previously proposed ordered structural models [25,52–55] are lower in energy than the disorder configurations. But why it is hard to observe large-scale ordered structures of GOs in experiment? Several possible effects such as kinetic factors during growth process and configuration

entropy must be taken into account. Since formation of GO through oxidation of graphene is an exothermic process, the functional groups can be easily added onto the graphene sheet. In the initial stage of growth, functional groups prefer to aggregate along the direction with lower growth barrier that is determined by the chemical environment of the existing groups on the GO layer. While considering the kinetic factors during growth, there are high diffusion energy barriers (up to 2.89 eV) between local minima to prevent growing large ordered structures [72]. In other words, the ordered structural models predicted by the theoretical simulations are only the consequence of thermodynamic factors but are prevented by the kinetic factors during realistic synthesis condition. Besides, the effect of configuration entropy [73], which prefers the disordered structures with high probability and becomes more significant at higher temperature, may also contribute to the experimentally observed amorphous GO structures. Recently, GO samples with ordered wrinkles have been synthesized, which confirmed the ordered arrangement of epoxide groups [74]. With improvement of experimental technology, we anticipate that the large-scale ordered GO with different oxygen functional groups will be fabricated in the future.

4. Conclusions

A series of amorphous GO structures with different coverage rates and OH:O ratios were constructed by randomly adding epoxy and hydroxyl groups onto a perfect graphene supercell with 80 carbon atoms following some structural rules. Ordered GO structures with epoxy and hydroxyl chains along the armchair direction were considered for comparison. The main conclusions from our first-principles computations are itemized as follows.

First, the thermodynamically stable amorphous GO is usually disordered in long range but exhibit some short-range ordered motif to stabilize the structures. The ordered structural models proposed by the previous theoretical calculations are more energetically favorable than the present amorphous ones. Since dealing with periodic supercells without edges and hole defects, here we only considered epoxide and hydroxyl, which are the dominant groups on graphene basal plane. However, in the realistic GO samples, there may exist some other groups, such as carboxyl and ketone; and these groups will most likely locate at the edges and hole defects. In addition, our present results are limited by the finite size effect of simulation supercell and zero-temperature in DFT optimization. In reality, at finite temperatures, migration and transformation of different functional groups may occur and the effects of kinetic factor and configuration entropy must be taken into account. This may answer the inconsistency between the experiments and theoretical predictions about the atomic structures of GOs.

Second, the amorphous GO structures exhibit reasonable thermodynamic stability and can be as stable as the ordered ones as the coverage rate is below 5%, which may correspond to the cases of reduced GO.

Third, the electronic properties of GOs can be effectively tailored by varying the concentration and/or relative ratio of epoxy and hydroxyl groups. The electrical conductivity of GOs will be enhanced by either lowering the coverage rate or increasing the relative ratio of epoxy groups.

The present theoretical results shed some lights on the atomic structures of GOs and suggest some possible ways of controlling the electronic properties of GO materials.

Acknowledgements

This work is supported in China by the Fundamental Research Funds for the Central Universities of China (No. DUT10ZD211) and the National Natural Science Foundation of China (No. 11134005), and in USA by NSF Grant EPS-1010094 and the Environmental Protection Agency (EPA Grant No. RD-83385601).

REFERENCES

[1] Novoselov KS, Geim AK, Morozov SV, Jiang D, Zhang Y, Dubonos SV, et al. Electric field effect in atomically thin carbon films. Science 2004;306(5696):666–9.
[2] Novoselov KS, Geim AK, Morozov SV, Jiang D, Katsnelson MI, Grigorieva IV, et al. Two-dimensional gas of massless Dirac fermions in graphene. Nature (London) 2005;438(7065):197–200.
[3] Stankovich S, Dikin DA, Dommett GHB, Kohlhaas KM, Zimney EJ, Stach EA, et al. Graphene-based composite materials. Nature (London) 2006;442(7100):282–6.
[4] Geim AK, Novoselov KS. The rise of graphene. Nat Mater 2007;6(3):183–91.
[5] Pereira JM, Vasilopoulos P, Peeters FM. Tunable quantum dots in bilayer graphene. Nano Lett 2007;7(4):946–9.
[6] Wu J, Pisula W, Mullen K. Graphenes as potential material for electronics. Chem Rev 2007;107(3):718–47.
[7] Stoller MD, Park S, Zhu Y, An J, Ruoff RS. Graphene-based ultracapacitors. Nano Lett 2008;8(10):3498–502.
[8] Brodie BC. On the atomic weight of graphite. Philos Trans R Soc Lond 1859;149:249–59.
[9] McAllister MJ, Li JL, Adamson DH, Schniepp HC, Abdala AA, Liu J, et al. Single sheet functionalized graphene by oxidation and thermal expansion of graphite. Chem Mater 2007;19(18):4396–404.
[10] Allen MJ, Tung VC, Kaner RB. Honeycomb carbon: a review of graphene. Chem Rev 2010;110(1):132–45.
[11] Park S, Ruoff RS. Chemical methods for the production of graphenes. Nat Nanotechnol 2009;4(4):217–24.
[12] Tung VC, Allen MJ, Yang Y, Kaner RB. High-throughput solution processing of large-scale graphene. Nat Nanotechnol 2009;4(1):25–9.
[13] Dreyer DR, Park S, Bielawski CW, Ruoff RS. The chemistry of graphene oxide. Chem Soc Rev 2010;39(1):228–40.
[14] Gomez-Navarro C, Weitz RT, Bittner AM, Scolari M, Mews A, Burghard M, et al. Electronic transport properties of individual chemically reduced graphene oxide sheets. Nano Lett 2007;7(11):3499–503.
[15] Becerril HA, Mao J, Liu Z, Stoltenberg RM, Bao Z, Chen Y. Evaluation of solution-processed reduced graphene oxide films as transparent conductors. ACS Nano 2008;2(3):463–70.
[16] Eda G, Fanchini G, Chhowalla M. Large-area ultrathin films of reduced graphene oxide as a transparent and flexible electronic material. Nat Nanotechnol 2008;3(5):270–4.
[17] Wu X, Sprinkle M, Li X, Ming F, Berger C, de Heer WA. Epitaxial-graphene/graphene-oxide junction: an essential

step towards epitaxial graphene electronics. Phys Rev Lett 2008;101(2):026801–4.
[18] Robinson JT, Perkins FK, Snow ES, Wei Z, Sheehan PE. Reduced graphene oxide molecular sensors. Nano Lett 2008;8(10):3137–40.
[19] Fowler JD, Allen MJ, Tung VC, Yang Y, Kaner RB, Weiller BH. Practical chemical sensors from chemically derived graphene. ACS Nano 2009;3(2):301–6.
[20] Liu Z, Wang Y, Zhang X, Xu Y, Chen Y, Tian J. Nonlinear optical properties of graphene oxide in nanosecond and picosecond regimes. Appl Phys Lett 2009;94(2):021902–3.
[21] Luo Z, Vora PM, Mele EJ, Johnson ATC, Kikkawa JM. Photoluminescence and band gap modulation in graphene oxide. Appl Phys Lett 2009;94(11):111903–9.
[22] Zhou Y, Bao Q, Tang LAL, Zhong Y, Loh KP. Hydrothermal dehydration for the "Green" reduction of exfoliated graphene oxide to graphene and demonstration of tunable optical limiting properties. Chem Mater 2009;21(13):2950–6.
[23] Ghosh S, Sarker BK, Chunder A, Zhai L, Khondaker SI. Position dependent photodetector from large area reduced graphene oxide thin films. Appl Phys Lett 2010;96(16):163103–9.
[24] Zhao B, Cao B, Zhou W, Li D, Zhao W. Nonlinear optical transmission of nanographene and its composites. J Phys Chem C 2010;114(29):12517–23.
[25] Wang L, Lee K, Sun YY, Lucking M, Chen ZF, Zhao JJ, et al. Graphene oxide as an ideal substrate for hydrogen storage. ACS Nano 2009;3(10):2995–3000.
[26] Xu J, Wang K, Zu SZ, Han BH, Wei Z. Hierarchical nanocomposites of polyaniline nanowire arrays on graphene oxide sheets with synergistic effect for energy storage. ACS Nano 2010;4(9):5019–26.
[27] Ramanathan T, Abdala AA, Stankovich S, Dikin DA, Herrera Alonso M, Piner RD, et al. Functionalized graphene sheets for polymer nanocomposites. Nat Nanotechnol 2008;3(6):327–31.
[28] Hontoria-Lucas C, Lopez-Peinado AJ, Lopez-Gonzalez JDD, Rojas-Cervantes ML, Martin-Aranda RM. Study of oxygen-containing groups in a series of graphite oxides: physical and chemical characterization. Carbon 1995;33(11):1585–92.
[29] He H, Riedl T, Lerf A, Klinowski J. Solid-state NMR studies of the structure of graphite oxide. J Phys Chem 1996;100(51):19954–8.
[30] Lerf A, He H, Riedl T, Forster M, Klinowski J. ^{13}C and ^{1}H MAS NMR studies of graphite oxide and its chemically modified derivatives. Solid State Ionics 1997;101–103(Pt 2):857–62.
[31] He H, Klinowski J, Forster M, Lerf A. A new structural model for graphite oxide. Chem Phys Lett 1998;287(1–2):53–6.
[32] Lerf A, He H, Forster M, Klinowski J. Structure of graphite oxide revisited. J Phys Chem B 1998;102(23):4477–82.
[33] Hummers WS, Offeman RE. Preparation of graphitic oxide. J Am Chem Soc 1958;80(6):1339.
[34] Szabo T, Berkesi O, Forgo P, Josepovits K, Sanakis Y, Petridis D, et al. Evolution of surface functional groups in a series of progressively oxidized graphite oxides. Chem Mater 2006;18(11):2740–9.
[35] Stankovich S, Dikin DA, Piner RD, Kohlhaas KA, Kleinhammes A, Jia Y, et al. Synthesis of graphene-based nanosheets via chemical reduction of exfoliated graphite oxide. Carbon 2007;45(7):1558–65.
[36] Jeong HK, Lee YP, Lahaye R, Park MH, An KH, Kim IJ, et al. Evidence of graphitic AB stacking order of graphite oxides. J Am Chem Soc 2008;130(4):1362–6.
[37] Gao W, Alemany LB, Ci LJ, Ajayan PM. New insights into the structure and reduction of graphite oxide. Nat Chem 2009;1(5):403–8.
[38] Mkhoyan KA, Contryman AW, Silcox J, Stewart DA, Eda G, Mattevi C, et al. Atomic and electronic structure of graphene-oxide. Nano Lett 2009;9(3):1058–63.
[39] Gomez-Navarro C, Meyer JC, Sundaram RS, Chuvilin A, Kurasch S, Burghard M, et al. Atomic structure of reduced graphene oxide. Nano Lett 2010;10(4):1144–8.
[40] Erickson K, Erni R, Lee Z, Alem N, Gannett W, Zettl A. Determination of the local chemical structure of graphene oxide and reduced graphene oxide. Adv Mater 2010;22(40):4467–72.
[41] Fan XB, Peng WC, Li Y, Li XY, Wang SL, Zhang GL, et al. Deoxygenation of exfoliated graphite oxide under alkaline conditions: a green route to graphene preparation. Adv Mater 2008;20(23):4490–3.
[42] Liu L, Ryu SM, Tomasik MR, Stolyarova E, Jung N, Hybertsen MS, et al. Graphene oxidation: thickness-dependent etching and strong chemical doping. Nano Lett 2008;8(7): 1965–70.
[43] Yang D, Velamakanni A, Bozoklu G, Park S, Stoller M, Piner RD, et al. Chemical analysis of graphene oxide films after heat and chemical treatments by X-ray photoelectron and Micro-Raman spectroscopy. Carbon 2009;47(1):145–52.
[44] Li X, Wang H, Robinson JT, Sanchez H, Diankov G, Dai H. Simultaneous nitrogen doping and reduction of graphene oxide. J Am Chem Soc 2009;131(43):15939–44.
[45] Kudin KN, Ozbas B, Schniepp HC, Prud'homme RK, Aksay IA, Car R. Raman spectra of graphite oxide and functionalized graphene sheets. Nano Lett 2008;8(1):36–41.
[46] Cai W, Piner RD, Stadermann FJ, Park S, Shaibat MA, Ishii Y, et al. Synthesis and solid-state NMR structural characterization of ^{13}C-labeled graphite oxide. Science 2008;321(5897):1815–7.
[47] Hofmann U, Holst R. Uber die saurenatur und die methylierung von graphitoxyd. Ber Dtsch Chem Ges 1939;72(4):754–71.
[48] Ruess G. Uber das graphitoxyhydroxyd (graphitoxyd). Monatsch Chem 1947;76(3):381–417.
[49] Scholz W, Boehm HP. Untersuchungen am graphitoxid. VI. Betrachtungen zur struktur des graphitoxids. Z Anorg Allg Chem 1969;369(3–6):327–40.
[50] Nakajima T, Mabuchi A, Hagiwara R. A new structure model of graphite oxide. Carbon 1988;26(3):357–61.
[51] Nakajima T, Matsuo Y. Formation process and structure of graphite oxide. Carbon 1994;32(3):469–75.
[52] Yan JA, Xian LD, Chou MY. Structural and electronic properties of oxidized graphene. Phys Rev Lett 2009;103(8):086802–4.
[53] Yan JA, Chou MY. Oxidation functional groups on graphene: structural and electronic properties. Phys Rev B 2010;82(12):125403–10.
[54] Wang L, Sun YY, Lee K, West D, Chen ZF, Zhao JJ, et al. Stability of graphene oxide phases from first-principles calculations. Phys Rev B 2010;82(16):161404–6.
[55] Zhang W, Carravetta V, Li Z, Luo Y, Yang J. Oxidation states of graphene: insights from computational spectroscopy. J Chem Phys 2009;131(24):244505–6.
[56] Xiang HJ, Wei SH, Gong XG. Structural motifs in oxidized graphene: a genetic algorithm study based on density functional theory. Phys Rev B 2010;82(3):035415–6.
[57] Lu N, Huang Y, Li HB, Li ZY, Yang JL. First principles nuclear magnetic resonance signatures of graphene oxide. J Chem Phys 2010;133(3):034502–7.
[58] Buchsteiner A, Lerf A, Pieper J. Water dynamics in graphite oxide investigated with neutron scattering. J Phys Chem B 2006;110(45):22328–38.
[59] Payne MC, Teter MP, Allan DC, Arias TA, Joannopoulos JD. Iterative minimization techniques for ab initio total-energy calculations: molecular dynamics and conjugate gradients. Rev Mod Phys 1992;64(4):1045–97.
[60] Segall MD, Lindan PJD, Probert MJ, Pickard CJ, Hasnip PJ, CS J, et al. First-principles simulation: ideas, illustrations and

the CASTEP code. J Phys: Condens Matter 2002;14(11):2717–44.
[61] Perdew JP, Burke K, Ernzerhof M. Generalized gradient approximation made simple. Phys Rev Lett 1996;77(18):3865–8.
[62] Hamann DR, Schluter M, Chiang C. Norm-conserving pseudopotentials. Phys Rev Lett 1979;43(20):1494–7.
[63] Monkhorst HJ, Pack JD. Special points for Brillouin-zone integrations. Phys Rev B 1976;13(12):5188–92.
[64] Baraket M, Walton SG, Wei Z, Lock EH, Robinson JT, Sheehan P. Reduction of graphene oxide by electron beam generated plasmas produced in methane/argon mixtures. Carbon 2010;48(12):3382–90.
[65] Boukhvalov DW, Katsnelson MI. Modeling of graphite oxide. J Am Chem Soc 2008;130(32):10697–701.
[66] Muti M, Sharma S, Erdem A, Papakonstantinou P. Electrochemical monitoring of nucleic acid hybridization by single-use graphene oxide-based sensor. Electroanalysis 2011;23(1):272–9.
[67] Loh KP, Bao Q, Eda G, Chhowalla M. Graphene oxide as a chemically tunable platform for optical applications. Nat Chem 2010;2(12):1015–24.
[68] Jung I, Dikin DA, Piner RD, Ruoff RS. Tunable electrical conductivity of individual graphene oxide sheets reduced at “low” temperatures. Nano Lett 2008;8(12):4283–7.
[69] Belgacem H, Merazga A. Determination of the density of localized states in semiconductors from the pre-recombination transient photoconductivity. Solid-State Electron 2008;52(1):73–7.
[70] Chang H, Sun Z, Yuan Q, Ding F, Tao X, Yan F, et al. Thin film field-effect phototransistors from bandgap-tunable, solution-processed, few-layer reduced graphene oxide films. Adv Mater 2010;22(43):4872–6.
[71] Liu L, Gao H, Zhao J, Lu J. Quantum conductance of armchair carbon nanocoils: roles of geometry effects. Sci China Phys Mech Astron 2011;54(5):841–5.
[72] Lu N, Yin D, Li Z, Yang J. Structure of graphene oxide: thermodynamics versus kinetics. J Phys Chem C 2011;115(24):11991–5.
[73] Zhao J, Zhuang C, Jiang X. Structure and mechanical properties of cubic BC2N crystals within a random solid solution model. Diamond Relat Mater 2010;19(11):1419–22.
[74] Fujii S, Enoki T. Cutting of oxidized graphene into nanosized pieces. J Am Chem Soc 2010;132(29):10034–41.